

# Anisotropic electronic properties of $a$ -axis-oriented $\text{Sr}_2\text{IrO}_4$ epitaxial thin-films

J. Nichols, O. B. Korneta, J. Terzic, L. E. De Long, G. Cao, J. W. Brill, and S. S. A. Seo<sup>a)</sup>

*Department of Physics and Astronomy, University of Kentucky, Lexington, KY 40506, USA*

## Abstract

We have investigated the transport and optical properties along the  $c$ -axis of  $a$ -axis-oriented  $\text{Sr}_2\text{IrO}_4$  epitaxial thin-films grown on  $\text{LaSrGaO}_4$  (100) substrates. The  $c$ -axis resistivity is approximately one order of magnitude larger than that of the  $ab$ -plane. Optical absorption spectra with  $E \perp c$  polarization show both Ir  $5d$  intersite transitions and charge-transfer transitions (O  $2p$  to Ir  $5d$ ), while  $E // c$  spectra show only the latter. The structural anisotropy created by biaxial strain in  $a$ -axis-oriented thin-films also changes the electronic structure and gap energy. These  $a$ -axis-oriented, epitaxial thin-films provide a powerful tool to investigate the highly anisotropic electronic properties of  $\text{Sr}_2\text{IrO}_4$ .

PACS: 71.70.Ej, 68.60.Bs, 68.55.-a, 73.61.-r, 78.20.-e

<sup>a)</sup> E-mail: a.seo@uky.edu

A layered iridate compound,  $\text{Sr}_2\text{IrO}_4$ , which is an antiferromagnetic insulator ( $T_N \sim 240 \text{ K}$ ),<sup>1,2</sup> has recently attracted substantial interest due to its exotic electronic state. Coexisting electronic correlations and strong spin-orbit coupling of  $5d$  electrons has led to the formation of the  $J_{\text{eff}} = 1/2$  Mott state in  $\text{Sr}_2\text{IrO}_4$  (SIO-214).<sup>3</sup> Even though debate continues concerning its ground state (i.e., Mott insulator vs. Slater insulator<sup>4,5</sup>), this compound has unprecedented potential for electronic device applications. For example, unconventional superconductivity is theoretically predicted in doped SIO-214<sup>6</sup> and the strong spin-orbit interaction is expected to result in novel electronic states such as topological insulators<sup>7</sup> and Weyl semimetals.<sup>8,9</sup> Recently, SIO-214 thin films have been grown and characterized,<sup>10-12</sup> resulting in a better understanding of the underlying physics of SIO-214 and providing impetus for developing device applications. However, only  $c$ -axis-oriented SIO-214 thin films have been synthesized thus far, which limits experimental access primarily to in-plane ( $ab$ -plane) properties. Hence, thin film studies of SIO-214 have produced results that are quite similar to those obtained for bulk SIO-214 crystals, whose naturally cleaved surfaces are also  $ab$ -planes. Since characterization of the  $c$ -axis of a number of layered oxides have revealed important physical information (e.g., the pseudo-gap energies in high- $T_c$  cuprates<sup>13</sup>), the fabrication of SIO-214 thin films with large  $ac$ -planes (or  $bc$ -planes) will permit investigations of important physical properties that are not readily accessible in typical bulk crystals and  $c$ -axis-oriented thin films.

In this Letter, we report the structural, transport, and optical properties of  $a$ -axis-oriented SIO-214 thin films, whose large surfaces ( $5 \times 5 \text{ mm}^2$ ) are  $bc$ -planes (or  $ac$ -planes). We have grown  $a$ -axis-oriented SIO-214 epitaxial thin films on  $\text{LaSrGaO}_4$  (100) single-crystal substrates, where the [100]-direction is the surface-normal direction. In a similar study of layered  $3d$  transition-metal oxides,  $a$ -axis-oriented thin films were grown on  $\text{LaSrAlO}_4$  (100),<sup>14</sup> which has

the same  $K_2NiF_4$ -structure as  $LaSrGaO_4$  (LSGO). Due to differences in the tetragonal lattice parameters for SIO-214 (5.4979 Å and 25.798 Å)<sup>15</sup> and LSGO (3.852 Å and 12.68 Å),<sup>16</sup> the [110] and  $[\bar{1}10]$  directions of the SIO-214 thin films are parallel to the [100] and [010] directions of LSGO, respectively, and the thin film's  $c$ -axis lies parallel to the [001]-axis of the substrate, as schematically illustrated in Fig. 1. The [100], [010], and [001]-directions of the LSGO substrate are labeled as  $a$ ,  $b$ , and  $c$ , respectively, and we use this notation in the following paragraphs.

Since the lattice mismatches between the substrate and the SIO-214 thin films are calculated as  $-0.92\%$  and  $-1.73\%$  along the  $b$ - and  $c$ -axes (Table 1), there is biaxial compressive strain along the  $b$ - and  $c$ - axes of the thin films. We have measured the transport and optical properties along the  $ab$ -plane and the  $c$ -axis of the SIO-214 thin films, which clearly show its anisotropic insulating nature. In particular, the  $c$ -axis optical spectrum has no absorption peaks except for the charge-transfer transition peak (from O  $2p$  to Ir  $5d$ ) above 2 eV. Our observation confirms that the low-energy optical transitions that exist near 0.5 eV and 1.0 eV in SIO-214 are due to *inter-site* optical transitions between Ir  $5d$  orbitals that lie in the  $ab$ -plane.

We have grown  $a$ -axis-oriented, epitaxial SIO-214 thin films using a custom-built pulsed laser deposition system with *in-situ* reflection high-energy electron diffraction (RHEED) and *in-situ* optical spectroscopic ellipsometry.<sup>17</sup> Optimal growth parameters are oxygen partial pressure ( $P_{O_2}$ ) of 10 mTorr, substrate temperature of 700 °C, and laser (KrF excimer,  $\lambda = 248$  nm) fluence of 1.2 J/cm<sup>2</sup>. We have monitored the thin film growth using RHEED, which shows a “layer-by-layer + island” growth mode, presumably due to the large surface energy of the film. A total film thickness of about 20 nm has been estimated by using 4 to 5 oscillations of the RHEED specular spot intensity during the initial growth.

The structure of these  $a$ -axis-oriented, epitaxial SIO-214 thin films has been identified using X-ray diffraction. The (220) and (440) thin-film peaks are only visible very near to the (200) and (400) substrate peaks in the  $\theta$ - $2\theta$  scan in Fig. 2 (a), ensuring that the films have an  $a$ -axis orientation. The FWHM of the rocking curves of the thin-film diffraction peaks are less than  $0.07^\circ$  (data not shown) suggesting that the samples have good crystallinity. In addition, the  $bc$ -plane epitaxy has been confirmed by pole figures and  $\phi$ -scans (data not shown). In order to obtain lattice-strain information, X-ray reciprocal space maps have been measured near the (310) and (303)-reflections of the LSGO substrate for the  $ab$ - and  $ac$ -planes, respectively, as shown in Fig. 1(b) and 1(c). Note that there is biaxial compressive strain in the  $bc$ -plane resulting in the elongated  $a$ -axis of the SIO-214 thin film, even though strain relaxation easily occurs along the  $b$ -axis. The lattice parameters, lattice strain, and the Poisson ratio are summarized in Table 1. It is noteworthy that artificial  $ab$ -plane anisotropy has been created by biaxial lattice strain in this sample geometry, i.e. the  $a$ -axis lattice parameter is longer than the  $b$ -axis. Therefore, the  $a$ -axis-oriented, epitaxial SIO-214 thin films have orthorhombic rather than tetragonal structure.

Figure 3 shows the electrical resistivity of the SIO-214 thin films for two current orientations: Samples were sliced and patterned into bar shapes to measure the temperature-dependent resistivity along the  $b$ -axis ( $\rho_{ab}$ ) and  $c$ -axis ( $\rho_c$ ) using conventional four-probe methods. Insulating behavior is clearly evident in both directions; however, the  $c$ -axis resistivity is about an order of magnitude larger than the  $b$ -axis resistivity. This anisotropy is also present in the Arrhenius plot shown in Fig. 3(b), where the dashed lines are fits to  $\rho(T) = \rho_0 \exp(\Delta/2k_B T)$ , where  $\rho$ ,  $\rho_0$ ,  $\Delta$ , and  $k_B$  are the resistivity, proportionality constant, gap energy, and Boltzmann constant, respectively. Note that the values of  $\Delta$  are estimated to be 97 meV (77 meV) at high temperature and 27 meV (24 meV) at low temperature for current applied along the  $c$ -axis ( $b$ -

axis). A similar temperature-dependent behavior has been reported for bulk SIO-214 crystals, where the temperature dependence of the gap is primarily attributed to additional magnetic ordering below the magnetic transition temperature.<sup>18</sup>

Figure 4(a) shows optical absorption spectra of the SIO-214 thin films, which also exhibit anisotropy. The optical absorption coefficients are measured at room temperature with a Fourier-transform infrared spectrometer for energies in the range of 0.05 – 0.6 eV, and a grating-type spectrometer for energies in the range of 0.5 – 6 eV, using polarized incident light with  $E \perp c$  or  $E // c$ . A schematic illustration of the measurement setup is presented in the inset of Fig 4(a), where LSGO and SIO-214 are blue and red, respectively. Two absorption peaks at around 0.5 eV ( $\alpha$ ) and 1.0 eV ( $\beta$ ) are clearly visible in the  $E \perp c$  spectra, while no absorption peak is present at these energies in the  $E // c$  spectra. The  $\alpha$  and  $\beta$  peaks have been already observed in the  $ab$ -plane of SIO-214 bulk crystals<sup>19</sup> and  $c$ -axis-oriented thin films<sup>12</sup>. They are interpreted as Ir  $5d$  optical transitions between  $J_{\text{eff}} = 1/2$  and  $J_{\text{eff}} = 3/2$  states,<sup>3,20</sup> as schematically illustrated in Fig. 4(b). Note that the Ir  $5d$  optical transitions reflect electron hopping between Ir sites in the  $ab$ -plane. The absence of the  $\alpha$  and  $\beta$  peaks in the  $E // c$  optical spectrum confirms that inter-site optical transitions are forbidden in the  $E // c$  polarization (Fig. 4(c)). However, both the  $E \perp c$  and  $E // c$  spectra exhibit a relatively isotropic feature at around 3 eV (A) due to charge-transfer optical transitions from O  $2p$  states to Ir  $5d$  states.

Note that the optical peak widths of the  $\alpha$  and  $\beta$  transitions in the  $E \perp c$  spectrum are quite similar to those of SIO-214 thin films under isotropic  $ab$ -plane tensile strain with a compressed  $c$ -axis lattice. In the recent study of  $c$ -axis-oriented SIO-214 thin films (i.e., SIO-214  $c$ -axis

normal to substrate surface) deposited on various substrates with both *ab*-plane tensile and compressive strain,<sup>12</sup> the optical peak widths and positions exhibit a systematic dependence on lattice strain. The  $E_{\perp c}$  optical spectrum (Fig. 4(a)) is similar to that for *c*-axis-oriented SIO-214 thin films grown on SrTiO<sub>3</sub> (100) and GdScO<sub>3</sub> (110) substrates, which are under isotropic tensile strain in the *ab*-plane with a decreased *c*-axis lattice parameter. Since there is *ab*-plane anisotropy in the *a*-axis oriented thin films discussed in this letter (Table 1), it is hard to draw a concrete conclusion concerning these data. However, the similarity of these two spectra suggests that changes in the *c*-axis lattice parameter (involving elongation or flattening of IO<sub>6</sub> octahedra) play an important role in changing the electronic structure of SIO-214. It is also noteworthy that an optical gap energy ( $\Delta_{op}$ ) of about 0.2 eV is estimated from the onset of the  $E_{\perp c}$  optical absorption spectrum, which is approximately two-thirds of the values obtained in Refs.<sup>12</sup> and <sup>19</sup>. This optical gap suppression, which is not observed in *c*-axis-oriented SIO-214 thin films, might be related to the *ab*-plane anisotropy in *a*-axis-oriented SIO-214 thin films. Since it is not clear how the artificial *ab*-plane anisotropy, i.e., strain-induced, different *a*- and *b*-axes lattice parameters, distorts the IrO<sub>6</sub> octahedra in *a*-axis-oriented thin films, microscopic characterizations such as scanning transmission electron microscopy<sup>21,22</sup> and resonant X-ray diffraction<sup>23,24</sup> will provide additional important information.

In summary, we have synthesized *a*-axis-oriented, epitaxial SIO-214 thin films with artificial *ab*-plane anisotropy and a flattened *c*-axis lattice on LSGO (100) substrates. We have observed that these thin films are insulating along both the *b*- and *c*-axes, but the *c*-axis resistivity is an order of magnitude larger than the *b*-axis resistivity. We have observed optical absorption spectra where the two optical peaks at 0.5 eV and 1.0 eV are only observed for  $E_{\perp c}$ , which

supports the view that these peaks originate from inter-site Ir  $5d$  transitions. Since the large surface area ( $bc$ -plane) of these samples is orthogonal to the naturally cleaved surface of this compound, our sample geometry provides an important way to investigate the in-plane anisotropy and  $c$ -axis properties, which are not easily accessible in bulk crystals.

We appreciate Emily Bittle for her help with the FT-IR measurements. This research was supported by the NSF through Grant Nos. EPS-0814194 (the Center for Advanced Materials), DMR-1262261 (JWB), DMR-0856234 (GC), DMR-1265162 (GC), by U.S. DoE through Grant No. DE-FG02-97ER45653 (LED), and by the Kentucky Science and Engineering Foundation with the Kentucky Science and Technology Corporation through Grant Agreement No. KSEF-148-502-12-303 (SSAS).

Table 1. Lattice parameters and strain of *a*-axis-oriented epitaxial thin films of Sr<sub>2</sub>IrO<sub>4</sub> (SIO-214).

	Crystallographic direction	LSGO lattice parameters (Å)	SIO-214 film pseudo-cubic lattice parameters (Å)	Lattice mismatch (%) <sup>*</sup>	Lattice strain (%) <sup>**</sup>
<i>a</i>	[100] <sub>sub</sub> // [110] <sub>film</sub>	3.852	3.91	—	+ 0.65
<i>b</i>	[010] <sub>sub</sub> // [ $\bar{1}$ 10] <sub>film</sub>	3.852	3.88	- 0.92	- 0.1
<i>c</i>	[001] <sub>sub</sub> // [001] <sub>film</sub>	12.68	12.7	- 1.73	- 1.4

<sup>\*</sup> Lattice mismatch is calculated from the pseudo-cubic lattice parameters of bulk SIO-214 ( $d_{\text{bulk}}$ ) and substrates ( $d_{\text{sub}}$ ) by  $(d_{\text{sub}} - d_{\text{bulk}}) / d_{\text{sub}} \times 100$  (%).

<sup>\*\*</sup> Lattice strain is estimated by using  $\varepsilon = (d_{\text{film}} - d_{\text{bulk}}) / d_{\text{bulk}} \times 100$  (%).

Poisson's ratio,  $\nu = \varepsilon_a / (\varepsilon_a - \varepsilon_b - \varepsilon_c) = 0.30$ .



## Figure Captions

FIG. 1 Schematic diagram of the sample geometry with the  $a$ -axis-oriented SIO-214 thin-film grown on the LSGO (100) substrate, where the  $\text{IrO}_6$  octahedra are red and the Sr atoms are blue. The  $[110]$ ,  $[\bar{1}10]$ , and  $[001]$  directions of the SIO-214 thin film are parallel to the  $a$ :  $[100]$ ,  $b$ :  $[010]$ , and  $c$ :  $[001]$  directions of LSGO, respectively. The large colored arrows represent the direction of crystal strain: compressive (green) along the  $b$ - and  $c$ -axes and tensile (orange) along the  $a$ -axis.

FIG. 2 X-ray diffraction data for SIO-214 thin-films on LSGO: (a)  $\theta$ - $2\theta$  scan of a thin film for which the  $(l\bar{l}0)$  film peaks are clearly visible and confirm the  $a$ -axis orientation of the film. Reciprocal space maps of (b) the SIO-214 (420) film peak (black  $\times$ ) near the LSGO (310) substrate peak (white cross), and (c) the SIO-214 (336) film peak (black  $\times$ ) near the LSGO (303) substrate peak (white cross).

FIG. 3 (a) Temperature dependence of the electrical resistivity of a SIO-214 thin-film on LSGO for current applied along the  $b$ -axis (red) and  $c$ -axis (blue). (b) Arrhenius plot of the resistivity data, where the dashed lines are fits to  $\rho(T) = \rho_0 \exp(\Delta/2k_B T)$  for two distinct temperature regions.

FIG. 4 (a) The optical absorption coefficient for SIO-214 thin films on LSGO where the incident light is polarized such that  $E_{\perp c}$  (red) and  $E_{//c}$  (blue). Schematic band structure and optical transitions (arrows) for (b) the  $E_{\perp c}$  polarization and (c) the  $E_{//c}$  polarization. The dotted lines indicate the Fermi energy.

## References

- <sup>1</sup> G. Cao, J. Bolivar, S. McCall, J. E. Crow, and R. P. Guertin, *Phys. Rev. B* **57**, R11039 (1998).
- <sup>2</sup> B. J. Kim, H. Ohsumi, T. Komesu, S. Sakai, T. Morita, H. Takagi, and T. Arima, *Science* **323**, 1329 (2009).
- <sup>3</sup> B. J. Kim, H. Jin, S. J. Moon, J. Y. Kim, B. G. Park, C. S. Leem, J. Yu, T. W. Noh, C. Kim, S. J. Oh, J. H. Park, V. Durairaj, G. Cao, and E. Rotenberg, *Phys. Rev. Lett.* **101**, 076402 (2008).
- <sup>4</sup> R. Arita, J. Kuneš, A. V. Kozhevnikov, A. G. Eguiluz, and M. Imada, *Phys. Rev. Lett.* **108**, 086403 (2012).
- <sup>5</sup> D. Hsieh, F. Mahmood, D. H. Torchinsky, G. Cao, and N. Gedik, *Phys. Rev. B* **86**, 035128 (2012).
- <sup>6</sup> F. Wang and T. Senthil, *Phys. Rev. Lett.* **106**, 136402 (2011).
- <sup>7</sup> M. Z. Hasan and C. L. Kane, *Rev. Mod. Phys.* **82**, 3045 (2010).
- <sup>8</sup> D. Pesin and L. Balents, *Nat. Phys.* **6**, 376 (2010).
- <sup>9</sup> X. Wan, A. M. Turner, A. Vishwanath, and S. Y. Savrasov, *Phys. Rev. B* **83**, 205101 (2011).
- <sup>10</sup> J. S. Lee, Y. Krockenberger, K. S. Takahashi, M. Kawasaki, and Y. Tokura, *Phys. Rev. B* **85**, 035101 (2012).
- <sup>11</sup> C. Rayan Serrao, J. Liu, J. T. Heron, G. Singh-Bhalla, A. Yadav, S. J. Suresha, R. J. Paull, D. Yi, J. H. Chu, M. Trassin, A. Vishwanath, E. Arenholz, C. Frontera, J. Železný, T. Jungwirth, X. Marti, and R. Ramesh, *Phys. Rev. B* **87**, 085121 (2013).
- <sup>12</sup> J. Nichols, J. Terzic, E. G. Bittle, O. B. Korneta, L. E. De Long, J. W. Brill, G. Cao, and S. S. A. Seo, *Appl. Phys. Lett.* **102**, 141908 (2013).
- <sup>13</sup> C. C. Homes, T. Timusk, R. Liang, D. A. Bonn, and W. N. Hardy, *Phys. Rev. Lett.* **71**, 1645 (1993).
- <sup>14</sup> J. Matsuno, Y. Okimoto, M. Kawasaki, and Y. Tokura, *Phys. Rev. Lett.* **95**, 176404 (2005).
- <sup>15</sup> M. K. Crawford, M. A. Subramanian, R. L. Harlow, J. A. Fernandez-Baca, Z. R. Wang, and D. C. Johnston, *Phys. Rev. B* **49**, 9198 (1994).
- <sup>16</sup> I. Rüter and H. Müller-Buschbaum, *Zeitschrift für anorganische und allgemeine Chemie* **584**, 119 (1990).
- <sup>17</sup> J. H. Gruenewald, J. Nichols, and S. S. A. Seo, *Rev. Sci. Instrum.* **84**, 043902 (2013).
- <sup>18</sup> M. Ge, T. F. Qi, O. B. Korneta, D. E. De Long, P. Schlottmann, W. P. Crummett, and G. Cao, *Phys. Rev. B* **84**, 100402 (2011).
- <sup>19</sup> S. J. Moon, H. Jin, W. S. Choi, J. S. Lee, S. S. A. Seo, J. Yu, G. Cao, T. W. Noh, and Y. S. Lee, *Phys. Rev. B* **80**, 195110 (2009).
- <sup>20</sup> S. J. Moon, H. Jin, K. W. Kim, W. S. Choi, Y. S. Lee, J. Yu, G. Cao, A. Sumi, H. Funakubo, C. Bernhard, and T. W. Noh, *Phys. Rev. Lett.* **101**, 226402 (2008).
- <sup>21</sup> J. M. LeBeau, S. D. Findlay, L. J. Allen, and S. Stemmer, *Ultramicroscopy* **110**, 118 (2010).
- <sup>22</sup> J. Hwang, J. Y. Zhang, J. Son, and S. Stemmer, *Appl. Phys. Lett.* **100**, 191909 (2012).
- <sup>23</sup> P. R. Willmott, S. A. Pauli, R. Herger, C. M. Schlepütz, D. Martocchia, B. D. Patterson, B. Delley, R. Clarke, D. Kumah, C. Cionca, and Y. Yacoby, *Phys. Rev. Lett.* **99**, 155502 (2007).

- <sup>24</sup> D. P. Kumah, A. Riposan, C. N. Cionca, N. S. Hussein, R. Clarke, J. Y. Lee, J. M. Millunchick, Y. Yacoby, C. M. Schlepütz, M. Björck, and P. R. Willmott, *Appl. Phys. Lett.* **93**, 081910 (2008).

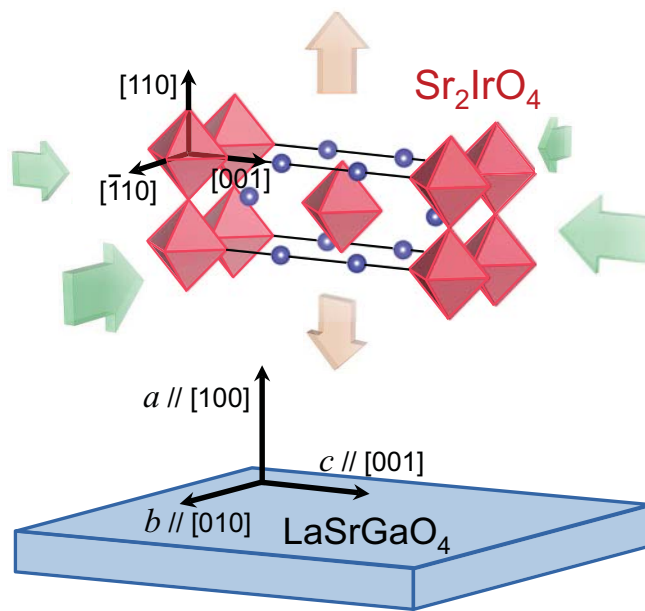


Figure 1  
Nichols *et al.*

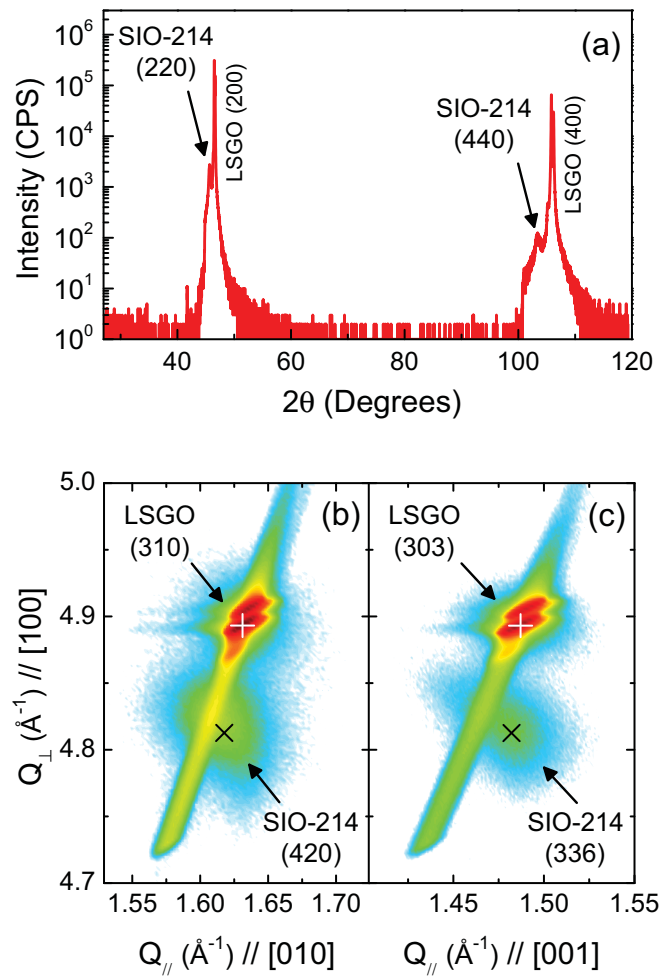


Figure 2  
Nichols *et al.*

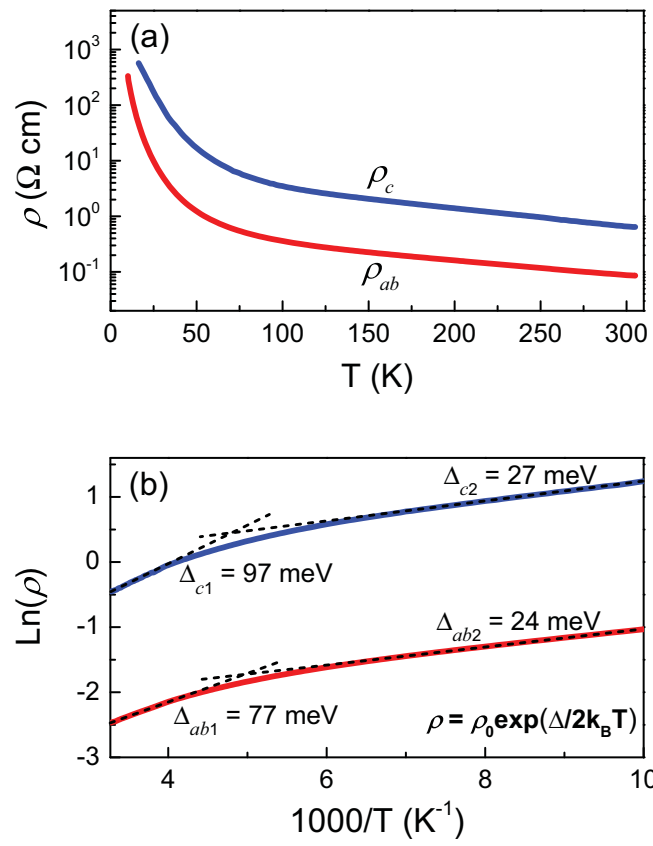


Figure 3  
Nichols *et al.*

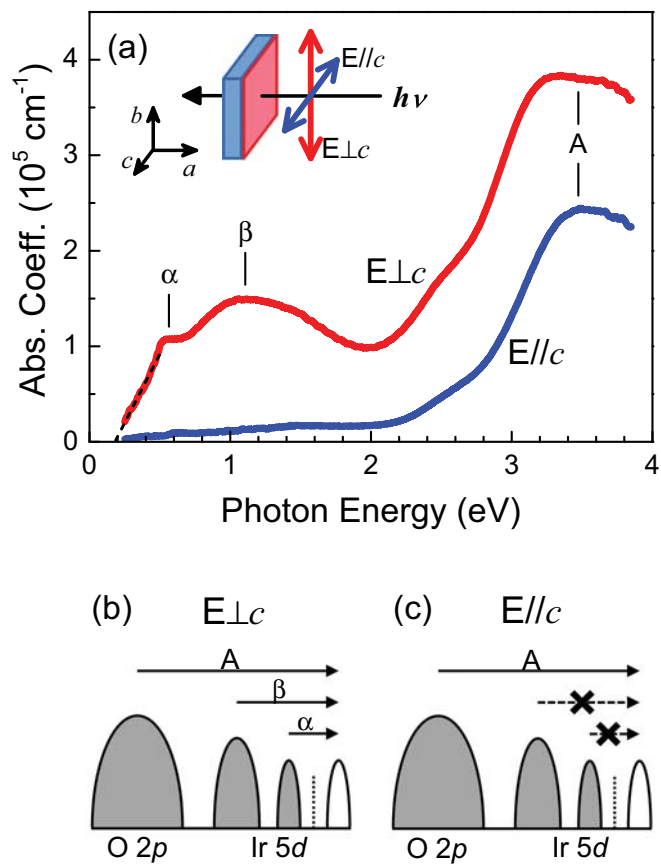


Figure 4  
Nichols *et al.*